

Butterfly: A Panacea for All Difficulties in Wildly Unsupervised Domain Adaptation

Feng Liu^{1,2} Jie Lu¹ Bo Han² Gang Niu²
Guangquan Zhang¹ Masashi Sugiyama^{2,3}

¹Center for Artificial Intelligence, University of Technology Sydney, Australia

²Center for Advanced Intelligence Project, RIKEN, Japan

³Graduate School of Frontier Sciences, University of Tokyo, Japan

feng.liu-2@student.uts.edu.au, {jie.lu, guangquan.zhang}@uts.edu.au
{bo.han, gang.niu}@riken.jp, sugi@k.u-tokyo.ac.jp

Abstract. In *unsupervised domain adaptation* (UDA), classifiers for the *target domain* (TD) are trained with *clean* labeled data from the *source domain* (SD) and unlabeled data from TD. However, in the wild, it is hard to acquire a large amount of perfectly clean labeled data in SD given limited budget. Hence, we consider a new, more realistic and more challenging problem setting, where classifiers have to be trained with *noisy* labeled data from SD and unlabeled data from TD—we name it *wildly UDA* (WUDA). We show that WUDA provably ruins all UDA methods if taking no care of label noise in SD, and to this end, we propose a *Butterfly* framework, a panacea for all difficulties in WUDA. Butterfly maintains four models (e.g., deep networks) simultaneously, where two take care of all adaptations (i.e., noisy-to-clean, labeled-to-unlabeled, and SD-to-TD-distributional) and then the other two can focus on classification in TD. As a consequence, Butterfly possesses all the necessary components for all the challenges in WUDA. Experiments demonstrate that under WUDA, Butterfly significantly outperforms existing baseline methods.

1 Introduction

Domain adaptation (DA) aims to learn a discriminative classifier in the presence of a shift between training data in source domain and test data in target domain [2,6,33,35,36]. Currently, DA can be divided into three categories: *supervised DA* [30], *semi-supervised DA* [14] and *unsupervised DA* (UDA) [25]. When the number of labeled data is few in target domain, supervised DA is also known as *few-shot DA* [24]. Since unlabeled data in target domain can be easily obtained, UDA exhibits the greatest potential in the real world [6,7,9,11,22,25,26].

UDA methods train with clean labeled data in source domain (i.e., clean source data) and unlabeled data in target domain (i.e., unlabeled target data) to obtain classifiers for the target domain, which mainly consist of three orthogonal techniques: *integral probability metrics* (IPM) [8,11,12,18,22], *adversarial training* [7,10,16,20,26,31] and *pseudo labeling* [25]. Compared to IPM- and adversarial-training-based methods, the pseudo-labeling-based method (i.e., *asymmetric tri-training domain adaptation* (ATDA) [25]) can construct a high-quality target-specific representation, providing a better classification performance. Besides, ATDA has been theoretically justified [25].

However, in the wild, the data volume of source domain tends to be large. To avoid the expensive labeling cost, labeled data in source domain normally come from amateur annotators or the Internet [19,27,29]. This brings us a new, more realistic and more challenging problem, *wildly unsupervised domain adaptation* (abbreviated as WUDA, Figure 1). This adaptation aims to transfer knowledge from noisy labeled data in source domain (\tilde{P}_s , i.e., noisy source data) to unlabeled target data (P_{x_t}). Unfortunately, existing UDA methods share an implicit assumption that *there are no noisy source data*. Namely, these methods focus on transferring knowledge from clean source data (P_s) to unlabeled target data (P_{x_t}). Therefore, these methods cannot well handle the WUDA.

In this paper, we theoretically reveal the deficiency of existing UDA methods. To improve these methods, a straightforward strategy is a two-step approach. In Figure 1, we can first use label-noise algorithms to train a model on noisy source data, then leverage this trained model to assign pseudo labels for noisy source data. Via UDA methods, we can transfer knowledge from pseudo-labeled source data (\hat{P}_s) to unlabeled target data (P_{x_t}). Nonetheless, pseudo-labeled source data are still noisy, and such two-step strategy may relieve but cannot eliminate noise effects.

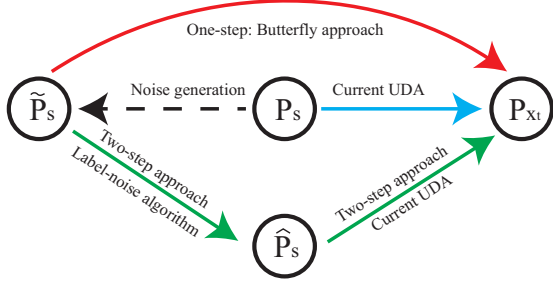


Fig. 1. Wildly unsupervised domain adaptation (WUDA).

The blue line denotes that UDA transfers knowledge from clean source data (P_s) to unlabeled target data (P_{x_t}). However, perfectly clean data is hard to acquire. This brings *wildly unsupervised domain adaptation* (WUDA), namely transferring knowledge from noisy source data (\tilde{P}_s) to unlabeled target data (P_{x_t}). Note that noise generation process (black dash line) is unknown in practice. To handle WUDA, a compromise solution is a two-step approach (green line), which sequentially combines label-noise algorithms ($\tilde{P}_s \rightarrow \hat{P}_s$) and existing UDA ($\hat{P}_s \rightarrow P_{x_t}$). This paper proposes a robust one-step approach called *Butterfly* (red line, $\tilde{P}_s \rightarrow P_{x_t}$ directly), which eliminates noise effects from \tilde{P}_s .

To circumvent the issue of two-step approach, under the theoretical guidance, we present a robust one-step approach called *Butterfly*. In high level, *Butterfly* directly transfers knowledge from \tilde{P}_s to P_{x_t} , and uses the transferred knowledge to construct target-specific representations. In low level, *Butterfly* maintains four networks dividing two branches (Figure 2): Two networks in Branch-I are jointly trained on noisy source data and pseudo-labeled target data (data in mixture domain); while two networks in Branch-II are trained on pseudo-labeled target data.

The reason why *Butterfly* can be robust takes root in the *dual-checking* principle: *Butterfly* checks high-correctness data out, from not only the data in mixture domain but also the pseudo-labeled target data. After cross-propagating these high-correctness data, *Butterfly* can obtain high-quality *domain-invariant representations* (DIR) and *target-specific representations* (TSR) simultaneously in an iterative manner. If we only check data in the mixture domain (i.e., single checking), the error existed in pseudo-labeled target data will accumulate, leading to low-quality DIR and TSR.

We conduct experiments on simulated WUDA tasks, including 4 *MNIST-to-SYND* tasks, 4 *SYND-to-MNIST* tasks and 24 *human-sentiment* tasks. Besides, we conduct experiments on 3 real-world WUDA tasks. Empirical results demonstrate that *Butterfly* can robustly transfer knowledge from noisy source data to unlabeled target data. Meanwhile, *Butterfly* performs much better than existing UDA methods when source domain suffers the extreme (e.g., 45%) noise.

2 Wildly unsupervised domain adaptation

In this section, we first define the new problem setting, and then analyze why it is so difficult.

2.1 Problem setting

We use following notations in this section: 1) a space $\mathcal{X} \subset \mathbb{R}^d$ and $\mathcal{Y} = \{1, 2, \dots, K\}$ as a label set; 2) $\tilde{p}_s(x_s, \tilde{y}_s)$, $p_s(x_s, y_s)$ and $q_s(x_s, y_s)$ represent densities of noisy, correct and incorrect multivariate random variables (m.r.v.) defined on $\mathcal{X} \times \mathcal{Y}$, respectively¹, and $\tilde{p}_{x_s}(x_s)$, $p_{x_s}(x_s)$ and $q_{x_s}(x_s)$ are their marginal densities; and 3) $p_{x_t}(x_t)$ represents density of m.r.v. x_t defined on \mathcal{X} ; and 4) we use $\ell(h(x), h'(x))$ to represent loss function between two labelling functions; and 5) we use $\tilde{R}_s(h) = \mathbb{E}_{\tilde{p}_s(x_s, \tilde{y}_s)}[\ell(h(x_s), \tilde{y}_s)]$ and $R_s(h) = \mathbb{E}_{p_s(x_s, y_s)}[\ell(h(x_s), y_s)]$ to represent expected risks on the noisy and correct m.r.v.; and 6) we use $\tilde{R}_s(h, h') = \mathbb{E}_{\tilde{p}_{x_s}(x_s)}[\ell(h(x_s), h'(x_s))]$, $R_s(h, h') = \mathbb{E}_{p_{x_s}(x_s)}[\ell(h(x_s), h'(x_s))]$ and $R_t(h, h') = \mathbb{E}_{p_{x_t}(x_t)}[\ell(h(x_t), h'(x_t))]$ to represent expected discrepancy between two labelling functions h, h' under different marginal densities; 7) the ground-truth and pseudo labeling function of the target domain are denoted by $f_t(x_t)$ and $\tilde{f}_t(x_t)$.

We formally define the new adaptation as follows.

Definition 1 (Wildly Unsupervised Domain Adaptation) Let X_t be a multivariate random variable defined on the space \mathcal{X} with respective a probability density p_{x_t} , where $p_{x_t} \neq p_{x_s}$. Given

¹ There are two common ways to express the density of noisy m.r.v. (Appendix A). One way is to use a mixture of densities of correct and incorrect m.r.v..

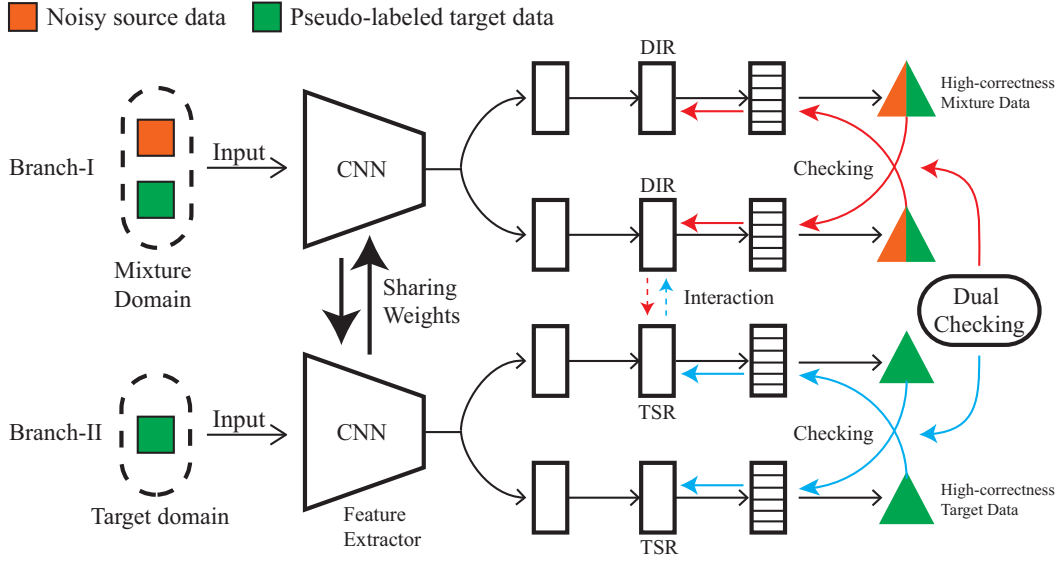


Fig. 2. Butterfly Framework.

i.i.d. data $\tilde{D}_s = \{(x_{si}, \tilde{y}_{si})\}_{i=1}^{n_s}$ and $D_t = \{x_{ti}\}_{i=1}^{n_t}$ drawn from \tilde{P}_s and P_{x_t} , a wildly unsupervised domain adaptation aims to train with \tilde{D}_s and D_t to accurately annotate each x_{ti} .

In Definition 1, \tilde{D}_s is noisy source data, D_t is unlabeled target data, and \tilde{P}_s and P_{x_t} are two probability measures corresponding to densities $\tilde{p}_s(x_s, \tilde{y}_s)$ and $p_{x_t}(x_t)$. Please note that *all proofs are demonstrated in Appendix H*.

2.2 WUDA provably ruins all UDA methods

Theoretically, we analyze why existing UDA methods cannot well transfer useful knowledge from noisy source data \tilde{D}_s to unlabeled target data D_t directly. We first present a theorem to show relations between $R_s(h)$ and $\tilde{R}_s(h)$.

Theorem 1 For any labelling function $h : \mathcal{X} \rightarrow \mathcal{Y}$, if $\tilde{p}_s(x_s, \tilde{y}_s)$ is generated by a transition matrix Q as demonstrated in Appendix A.1, we have

$$\tilde{R}_s(h) = R_s(h) + \mathbb{E}_{p_{x_s}(x_s)}[\boldsymbol{\eta}^T(x_s)(Q - I)\boldsymbol{\ell}(h(x_s))], \quad (1)$$

where $\boldsymbol{\ell}(h(x_s)) = [\ell(h(x_s), 1), \dots, \ell(h(x_s), K)]^T$ and $\boldsymbol{\eta}(x_s) = [p_{Y_s|X_s}(1|x_s), \dots, p_{Y_s|X_s}(K|x_s)]^T$. If $\tilde{p}_s(x_s, \tilde{y}_s)$ is generated by sample selection as described in Appendix A.2, we have

$$\tilde{R}_s(h) = (1 - \rho)R_s(h) + \rho\mathbb{E}_{q_{x_s}(x_s)}[\boldsymbol{\eta}_q^T(x_s)\boldsymbol{\ell}(h(x_s))], \quad (2)$$

where $\boldsymbol{\eta}_q(x_s) = [q_{Y_s|X_s}(1|x_s), \dots, q_{Y_s|X_s}(K|x_s)]^T$.

Remark 1 In Eq. (2), $\mathbb{E}_{q_{x_s}(x_s)}[\boldsymbol{\eta}_q^T(x_s)\boldsymbol{\ell}(h(x_s))]$ represents the expected risk on the incorrect m.r.v.. To ensure that we can gain useful knowledge from \tilde{P}_s , we need to avoid $\tilde{R}_s(h) \approx \mathbb{E}_{q_{x_s}(x_s)}[\boldsymbol{\eta}_q^T(x_s)\boldsymbol{\ell}(h(x_s))]$. Specifically, we assume: there is a constant $0 < M_s < \infty$ such that $\mathbb{E}_{q_{x_s}(x_s)}[\boldsymbol{\eta}_q^T(x_s)\boldsymbol{\ell}(h(x_s))] \leq R_s(h) + M_s$.

Theorem 1 shows that the expected risk $\tilde{R}_s(h)$ only equals $R_s(h)$ when two cases happen: 1) $Q = I$ and $\rho = 0$ and 2) some special combinations (e.g., special p_{x_s} , q_{x_s} , Q , η and ℓ) to make the second

term in Eq. (1) equal zero or to make the second term in Eq. (2) equal $\rho R_s(h)$. Case 1) means that data in source domain is clean, which is not real in the wild. Case 2) almost never happens, since it is hard to find such special combinations when p_{x_s} , q_{x_s} , Q and η are unknown. Thus, $\tilde{R}_s(h)$ has an essential difference with $R_s(h)$. Then, we derive the upper bound of $R_t(h)$ as follows.

Theorem 2 For any labelling function $h : \mathcal{X} \rightarrow \mathcal{Y}$, we have

$$R_t(h, f_t) \leq \underbrace{\tilde{R}_s(h)}_{(i) \text{ risk on noisy data}} + \underbrace{|R_t(h, \tilde{f}_t) - \tilde{R}_s(h, \tilde{f}_t)|}_{(ii) \text{ discrepancy between distributions}} + \underbrace{|R_s(h, \tilde{f}_t) - R_s(h)|}_{(iii) \text{ domain dissimilarity}} \\ + \underbrace{|\tilde{R}_s(h) - R_s(h)| + |\tilde{R}_s(h, \tilde{f}_t) - R_s(h, \tilde{f}_t)|}_{(iv) \text{ noise effects from source } \Delta_s} + \underbrace{|R_t(h, f_t) - R_t(h, \tilde{f}_t)|}_{(v) \text{ noise effects from target } \Delta_t}. \quad (3)$$

Remark 2 To ensure that we can gain useful knowledge from $\tilde{f}_t(x_t)$, we assume: there is a constant $0 < M_t < \infty$ such that $\mathbb{E}_{q_{x_s}(x)}[\ell(h(x), \tilde{f}_t(x))] \leq R_s(h, \tilde{f}_t) + M_t$ and $\mathbb{E}_{q_{x_t}(x)}[\ell(h(x), \tilde{f}_t(x))] \leq R_t(h, f_t) + M_t$, where $q_{x_t}(x) = p_{x_t}(x)1_A(x)/P_{x_t}(A)$ and $A = \{x : \tilde{f}_t(x) \neq f_t(x)\}$.

It is clear that the upper bound of $R_t(h, f_t)$, shown in (3), has 5 components. However, existing UDA methods only focus on minimizing (i) + (ii) [7,8,22] or (i) + (ii) + (iii) [25], which ignores terms (iv) and (v) (i.e., $\Delta = \Delta_s + \Delta_t$). Thus, in theory, existing UDA methods cannot handle wildly unsupervised domain adaptation well.

3 Two-step approach versus one-step approach

In this section, we first analyze the deficiency of two-step approach and then prove that one-step approach can eliminate noise effects under certain assumptions.

3.1 Two-step approach (a compromise solution)

To reduce noise effects from noisy source data, a straightforward way is to apply a two-step strategy. For example, we first use Co-teaching [15] to train a model with noisy source data, then these data are assigned pseudo labels using the trained model. Via ATDA approach, we can transfer knowledge from the pseudo-labeled source data to unlabeled target data.

Nonetheless, the pseudo-labeled source data is still noisy. Let labels of noisy source data \tilde{y}_s be replaced with pseudo labels \tilde{y}'_s after pre-processing. Noise effects Δ will become pseudo-label effects Δ_p as follows.

$$\Delta_p = \underbrace{|\tilde{R}'_s(h) - R_s(h)| + |\tilde{R}'_s(h, \tilde{f}_t) - R_s(h, \tilde{f}_t)|}_{\text{pseudo-label effects from source } \Delta'_s} + \Delta_t, \quad (4)$$

where $\tilde{R}'_s(h)$ and $\tilde{R}'_s(h, \tilde{f}_t)$ correspond to $\tilde{R}_s(h)$ and $\tilde{R}_s(h, \tilde{f}_t)$ in Δ_s . It is clear that the difference between Δ_p and Δ is $\Delta'_s - \Delta_s$. The first term in Δ'_s may be less than that in Δ_s due to Co-teaching, but the second term in Δ'_s may be higher than that in Δ_s since Co-teaching does not consider to minimize it. Thus, it is hard to say whether $\Delta'_s < \Delta_s$ (i.e., $\Delta_p < \Delta$). This means that, the two-step strategy may not really reduce noise effects.

3.2 One-step approach (a noise-eliminating solution)

To eliminate noise effects Δ , we aim to select correct data simultaneously from noisy source data and pseudo-labeled target data.

In theory, we prove that noise effects will be eliminated if we can select correct data with a high probability. Let ρ_{01}^s represent the probability that incorrect data is selected from noisy source data, and ρ_{01}^t represent the probability that incorrect data is selected from pseudo-labeled target data. Theorem 3 shows that $\Delta \rightarrow 0$ if $\rho_{01}^s \rightarrow 0$ and $\rho_{01}^t \rightarrow 0$ and presents a new upper bound of $R_t(h, f_t)$.

Theorem 3 Given two m.r.v. (X_s, Y_s, U_s) defined on $\mathcal{X} \times \mathcal{Y} \times \mathcal{V}$ and (X_t, U_t) defined on $\mathcal{X} \times \mathcal{V}$, under the assumptions in Remarks 1 and 2, $\forall \epsilon \in (0, 1)$, there are δ_s and δ_t , if $\mathbb{E}_{p'_{x_t}(x_t)}[\ell(h(x_t), f_t(x_t))] \leq R_t(h, f_t) + \rho_{01}^s M_t$, $\rho_{01}^s < \delta_s$ and $\rho_{01}^t < \delta_t$, for any labeling function h , we will have

$$|\tilde{R}_s^{p_0}(h, \tilde{f}_t, u_s) - R_s(h, \tilde{f}_t)| + |\tilde{R}_s^{p_0}(h, u_s) - R_s(h)| < 2\epsilon. \quad (5)$$

Moreover, if $\rho_{01}^s \leq \delta_s$ and $\rho_{01}^t \leq \delta_t$, we will have

$$\begin{aligned}
 R_t(h, f_t) \leq & \underbrace{\tilde{R}_s^{po}(h, u_s)}_{(i) \text{ risk on noisy data}} + \underbrace{|\tilde{R}_t^{po}(h, \tilde{f}_t, u_t) - \tilde{R}_s^{po}(h, \tilde{f}_t, u_s)|}_{(ii) \text{ discrepancy between distributions}} + \underbrace{|R_s(h, \tilde{f}_t) - R_s(h)|}_{(iii) \text{ domain dissimilarity}} \\
 & + \underbrace{2\epsilon}_{(iv) \text{ noise effects from source } \Delta_s} + \underbrace{2\epsilon}_{(v) \text{ noise effects from target } \Delta_t}, \tag{6}
 \end{aligned}$$

where

$$\begin{aligned}
 \tilde{R}_s^{po}(h, u_s) &= (1 - \rho_{u_s})^{-1} \mathbb{E}_{\tilde{p}_s^{po}(x_s, y_s, u_s)}[u_s \ell(h(x_s), y_s)], \\
 \tilde{R}_t^{po}(h, \tilde{f}_t, u_t) &= (1 - \rho_{u_t})^{-1} \mathbb{E}_{\tilde{p}_t^{po}(x_t, u_t)}[u_t \ell(h(x_t), \tilde{f}_t(x_t))], \\
 \tilde{R}_s^{po}(h, \tilde{f}_t, u_s) &= (1 - \rho_{u_s})^{-1} \mathbb{E}_{\tilde{p}_s^{po}(x_s, y_s, u_s)}[u_s \ell(h(x_s), \tilde{f}_t(x_s))],
 \end{aligned}$$

$p'_{x_t}(x) = p_{x_t}(x)1_B(x)/P_{x_t}(B)$, $\tilde{p}_s^{po}(x_s, y_s, u_s)$ is the density of (X_s, Y_s, U_s) , $\tilde{p}_t^{po}(x_t, u_t)$ is the density of (X_t, U_t) , $\rho_{u_s} = \int_{\mathcal{X}} \sum_{y_s=1}^K \tilde{p}_s^{po}(x_s, y_s, 0) dx_s < 1$, $\rho_{u_t} = \int_{\mathcal{X}} \tilde{p}_t^{po}(x_t, 0) dx_t < 1$, $B = \mathcal{X}/A$ and $\mathcal{V} = \{0, 1\}$.

Remark 3 In Appendix H.3, we give precise definitions of ρ_{01}^s and ρ_{01}^t and demonstrate the meaning of $\mathbb{E}_{p'_{x_t}(x_t)}[\ell(h(x_t), f_t(x_t))] \leq R_t(h, f_t) + \rho_{01}^s M_t$ (Remark 4).

Data drawn from the distribution of (X_s, Y_s, U_s) can be regarded as a pool that mixes the selected ($u_s = 1$) and unselected ($u_s = 0$) noisy source data. Data drawn from the distribution of (X_t, U_t) can be regarded as a pool that mixes the selected ($u_t = 1$) and unselected ($u_t = 0$) pseudo-labeled target data. Theorem 3 shows that if selected data have a high probability to be correct ones ($\rho_{01}^s \rightarrow 0$ and $\rho_{01}^t \rightarrow 0$), then Δ_s and Δ_t approach 0, meaning that noise effects are eliminated. This motivates us to find a reliable way to select correct data from noisy source data and pseudo-labeled target data and build up a one-step approach for WUDA.

4 Butterfly: Towards robust one-step approach

This section presents a robust one-step approach called Butterfly in details, and demonstrates how Butterfly minimizes all terms in the right side of Eq. (6).

4.1 Principled design of Butterfly

Guided by Theorem 3, a robust approach should check high-correctness data out (meaning $\rho_{01}^s \rightarrow 0$ and $\rho_{01}^t \rightarrow 0$). This checking process will make (iv) and (v), $2\epsilon + 2\epsilon$, become 0. Then, we can obtain gradients of $\tilde{R}_s^{po}(h, u_s)$, $\tilde{R}_s(h, \tilde{f}_t, u_s)$ and $\tilde{R}_t^{po}(h, \tilde{f}_t, u_t)$ w.r.t. parameters of h and use these gradients to minimize them, which minimizes (i) and (ii) as $(i) + (ii) \leq \tilde{R}_s^{po}(h, u_s) + \tilde{R}_s(h, \tilde{f}_t, u_s) + \tilde{R}_t^{po}(h, \tilde{f}_t, u_t)$. Note that (iii) cannot be directly minimized since we cannot pinpoint clean source data. However, following [25], we can indirectly minimize (iii) via minimizing $\tilde{R}_s^{po}(h, u_s) + \tilde{R}_s^{po}(h, \tilde{f}_t, u_s)$, as $(iii) \leq R_s(h, \tilde{f}_t) + R_s(h) \leq \tilde{R}_s^{po}(h, u_s) + \tilde{R}_s^{po}(h, \tilde{f}_t, u_s) + 2\epsilon$, where the last inequality follows (5). This means that a robust approach guided by Theorem 3 can minimize all terms in the right side of inequality in (6).

To realize this robust approach, we propose a Butterfly framework (Algorithm 2), which trains four networks dividing into two branches (Figure 2). By using dual-checking principle, Branch-I checks which data is correct in the mixture domain; while Branch-II checks which pseudo-labeled target data is correct. To ensure these checked data highly-correct, we apply the small-loss trick based on memorization effects of deep learning [1]. After cross-propagating these checked data [3], Butterfly can obtain high-quality DIR and TSR simultaneously in an iterative manner. Theoretically, Branch-I minimizes $(i) + (ii) + (iii) + (iv)$; while Branch-II minimizes $(ii) + (v)$. This means that Butterfly can minimize all terms in the right side of inequality in (6).

Algorithm 1 Checking($F_1, F_2, D, \eta, \alpha$)

1: Input networks F_1, F_2 , mini-batch D , learning rate η , remember rate α ;
2: Obtain $u_1 = \arg \min_{u'_1: 1u'_1 > \alpha|D|} \mathcal{L}(\theta_1, u'_1; F_1, D)$; // Check high-correctness data
3: Obtain $u_2 = \arg \min_{u'_2: 1u'_2 > \alpha|D|} \mathcal{L}(\theta_2, u'_2; F_2, D)$; // Check high-correctness data
4: Update $\theta_1 = \theta_1 - \eta \nabla \mathcal{L}(\theta_1, u_1; F_1, D)$; // Update θ_1
5: Update $\theta_2 = \theta_2 - \eta \nabla \mathcal{L}(\theta_2, u_2; F_2, D)$; // Update θ_2
6: Output F_1 and F_2

4.2 Loss function in Butterfly

Due to $\tilde{R}_s^{\text{po}}(h, u_s)$, $\tilde{R}_t^{\text{po}}(h, \tilde{f}_t, u_t)$ and $\tilde{R}_s^{\text{po}}(h, \tilde{f}_t, u_s)$ in Theorem 3, four networks trained by Butterfly share the same loss function but with different inputs.

$$\mathcal{L}(\theta, u; F, D) = \frac{1}{\sum_{i=1}^n u_i} \sum_{i=1}^n u_i \ell(F(x_i), \tilde{y}_i), \quad (7)$$

where n is the batch size, and F represents a network (e.g., F_1, F_2, F_{t1} and F_{t2}). $D = \{(x_i, \tilde{y}_i)\}_{i=1}^n$ is a mini-batch for training a network, where $\{x_i, \tilde{y}_i\}_{i=1}^n$ could be data in mixture domain or target domain (Figure 2), and θ represents parameters of F and $u = [u_1, \dots, u_n]^T$ is an n -by-1 vector whose elements equal 0 or 1. For two networks in Branch-I, following [25], we also add a regularizer $|\theta_{f11}^T \theta_{f21}|$ in their loss functions, where θ_{f11} and θ_{f21} are weights of the first fully-connect layer of F_1 and F_2 . With this regularizer, F_1 and F_2 will learn from different features.

4.3 Training procedure of Butterfly

For two networks in each branch, they will first check high-correctness data out and then cross update their parameters using these data. Algorithm 1 show how F_1 and F_2 (or F_{t1} and F_{t2}) check these data out and use checked data to update parameters of them.

Based on loss function defined in Eq. (7), the entire training procedure of Butterfly is shown in Algorithm 2. First, the algorithm initializes training data for two branches (\tilde{D} for Branch-I and \tilde{D}_t^l for Branch-II), four networks (F_1, F_2, F_{t1} and F_{t2}) and the number of pseudo labels (line 2). In the first epoch ($T = 1$), \tilde{D} and \tilde{D}_t^l are the same with \tilde{D}_s because there are only unlabeled target data. After mini-batch \tilde{D} is fetched from \tilde{D} (line 4), F_1 and F_2 check high-correctness data out and update their parameters using Algorithm 1 (lines 5). Using similar procedures, F_{t1} and F_{t2} can also update their parameters using Algorithm 1 (lines 6-7).

In each epoch, after N_{max} mini-batch updating, we randomly select n_t^l unlabeled target data and assign them pseudo labels using F_1 and F_2 (lines 8). Following [25], the Labeling function in Algorithm 2 (line 8) assigns pseudo labels for unlabeled target data, when predictions of F_1 and F_2 agree and at least one of them is confident about their predictions (probability above 0.9 or 0.95). Using this function, we can obtain the pseudo-labeled target data \tilde{D}_t^l for training Branch-II in the next epoch. Then, we merge \tilde{D}_t^l and \tilde{D}_s to be \tilde{D} for training Branch-I in the next epoch (line 9). Finally, we update n_t^l , $R(T)$ and $R_t(T)$ in lines 10-11 according to [25] and [15].

4.4 Relations to Co-teaching and TCL

Although Co-teaching [15] applies the small-loss trick and the cross-update technique to train deep networks against noisy data, it can only deal with one-domain problem instead cross-domain problem. Recalling definitions of Δ_s and Δ_t in (3), Co-teaching can only minimize the first term in Δ_s or Δ_t , and ignore the second term in Δ_s . This deficiency limits Co-teaching to eliminate noise effects $\Delta_s + \Delta_t$. However, Butterfly can naturally eliminate them. Recently, *transferable curriculum learning* (TCL) is a robust UDA method to handle noise [28]. TCL uses small-loss trick to train the *domain-adversarial neural network* (DANN) [7]. However, TCL can only minimize (i) + (ii) + (iv), while Butterfly can minimize all terms in the right side of (6).

Algorithm 2 Butterfly Framework: quadruple training for WUDA problem

1: Input \tilde{D}_s, D_t , learning rate η , fixed τ , fixed τ_t , epoch T_k and T_{max} , iteration N_{max} , # of pseudo-labeled target data n_{init} , max of n_{init} $n_{t,max}^l$;
2: Initial $F_1, F_2, F_{t1}, F_{t2}, \tilde{D}_t^l = \tilde{D}_s, \tilde{D} = \tilde{D}_s, n_t^l = n_{init}$;
for $T = 1, 2, \dots, T_{max}$ **do**
 3: Shuffle training set \tilde{D} ; // Noisy dataset
 for $N = 1, \dots, N_{max}$ **do**
 4: Fetch mini-batch \tilde{D} from \tilde{D} ;
 5: Update Branch-I: $F_1, F_2 = \text{Checking}(F_1, F_2, \tilde{D}, \eta, R(T))$; // Check mixture samples
 6: Fetch mini-batch \tilde{D}_t from \tilde{D}_t^l ;
 7: Update Branch-II: $F_{t1}, F_{t2} = \text{Checking}(F_{t1}, F_{t2}, \tilde{D}_t, \eta, R_t(T))$; // Check target samples
 end
 8: Obtain $\tilde{D}_t^l = \text{Labelling}(F_1, F_2, D_t, n_t^l)$; // Label D_t , following [25]
 9: Obtain $\tilde{D} = \tilde{D}_s \cup \tilde{D}_t^l$;
 10: Update $n_t^l = \min\{T/20 * n_t, n_{t,max}^l\}$;
 11: Update $R(T) = 1 - \min\{\frac{T}{T_k}\tau, \tau\}$, $R_t(T) = 1 - \min\{\frac{T}{T_k}\tau_t, \tau_t\}$;
end
12: Output F_{t1} and F_{t2}

5 Experiments

5.1 Simulated WUDA tasks

We verify the effectiveness of our approach on three benchmark datasets (vision and text), including *MNIST*, *SYN-DIGITS* (*SYND*) and *Amazon products reviews* (e.g., *book*, *dvd*, *electronics* and *kitchen*). They are used to construct 14 basic tasks: *MNIST*→*SYND* ($M \rightarrow S$), *SYND*→*MNIST* ($S \rightarrow M$), *book*→*dvd* ($B \rightarrow D$), *book*→*electronics* ($B \rightarrow E$), ... , and *kitchen* → *electronics* ($K \rightarrow E$). These tasks are often used for evaluation of UDA methods [7,25,26]. Since all source datasets are clean, we need to corrupt source datasets manually by a noise transition matrix Q [15,17], which can form simulated WUDA tasks. We assume that the matrix Q has two representative structures: 1) Symmetry flipping; 2) Pair flipping [15], which are defined in Appendix B.

The noise rate ρ is chosen from $\{0.2, 0.45\}$. Intuitively, $\rho = 0.45$ means almost over half of the noisy source data have wrong labels that cannot be learned without additional assumptions. $\rho = 0.2$ means only 20% labels are corrupted, which is a low-level noise situation. Note that pair case is much harder than symmetry case [15]. For each basic task, we have four kinds of noisy source data: *Pair*-45% (P45), *Pair*-20% (P20), *Symmetry*-45% (S45), *Symmetry*-20% (S20). Thus, we evaluate the performance of each method using 32 simulated WUDA tasks: 8 digit recognition tasks and 24 human-sentiment tasks. Note that the human-sentiment task is a binary classification problem, so pair flipping is equal to symmetry flipping. Thus, we only have 24 human-sentiment tasks. Results on human-sentiment tasks are reported in Appendix C.

5.2 Real-world WUDA tasks

We also verify the efficacy of our approach on “cross-dataset benchmark” including *Bing*, *Caltech256*, *Imagenet* and *SUN* [29]. In this benchmark, *Bing*, *Caltech256*, *Imagenet* and *SUN* contain common 40 classes. Since *Bing* dataset was formed by collecting images retrieved by Bing image search, it contains rich noisy data, with presence of multiple objects in the same image, polysemy and caricaturization [29]. We use *Bing* as noisy source data, and *Caltech256*, *Imagenet* and *SUN* as unlabeled target data, which can form three real-world WUDA tasks.

5.3 Baselines

We realize Butterfly using four networks (abbreviated as B-Net) and compare B-Net with following baselines: 1) ATDA: representative pseudo label based UDA method [25]; 2) *deep adaptation networks* (DAN): representative IPM based UDA method [22]; 3) DANN: representative adversarial training based UDA method [7]; 4) Co teaching+ATDA (Co+ATDA): a two-step method, which is a combination of the state-of-the-art label-noise algorithm (Co-teaching) [15] and UDA method

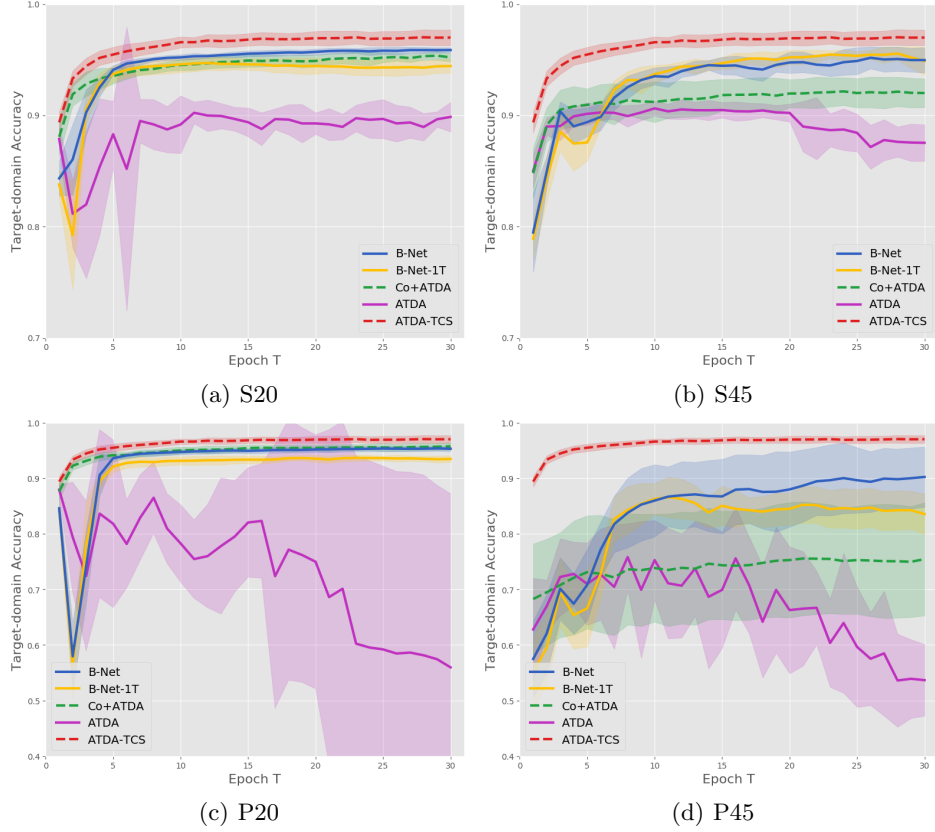


Fig. 3. Target-domain accuracy vs. number of epochs on four $SYND \rightarrow MNIST$ tasks.

(ATDA) [25]; 5) TCL: an existing robust UDA method; 6) *B-Net with 1 target-specific network* (B-Net-1T): without considering Δ_t (single-checking method). Note that ATDA is the most related UDA method compared to B-Net. Implementation details are demonstrated in Appendix D.

5.4 Results on simulated WUDA (including 8 tasks)

Table 1 reports the accuracy on the unlabeled target data in 8 tasks. As can be seen, on S20 case (the easiest case), most methods work well. ATDA has a satisfactory performance although it does not consider the noise effects explicitly. Then, when facing harder cases (i.e., P20 and P45), ATDA fails to transfer useful knowledge from noisy source data to unlabeled target data. On Pair-flip cases, the performance of ATDA is much lower than our methods. When facing hardest cases (i.e., $M \rightarrow S$ with P45 and S45), DANN has the higher accuracy than DAN and ATDA. However, when facing easiest cases (i.e., $S \rightarrow M$ with P20 and S20), the performance of DANN is worse than that of DAN and ATDA.

Although two-step method Co+ATDA outperforms ATDA in all 8 tasks, it cannot beat one-step methods (B-Net-1T and B-Net) in terms of average accuracy. This result is an evidence for the claim in Section 3. In Table 1, B-Net outperforms B-Net-1T in 7 out of 8 tasks. This reveals that pseudo-labeled target data indeed reduce the quality of TSR. Note that B-Net cannot outperform all methods in all tasks. In the task $S \rightarrow M$ with P20, Co+ATDA outperforms all methods (slightly higher than B-Net), since pseudo-labeled source data are almost correct. In the task $M \rightarrow S$ with S45, B-Net-1T outperforms all methods, including the second best B-Net. We conjecture that pseudo-labeled target data may contain much instance-dependence noise in this special case, where small-loss data may not be fully correct.

Figures 3 and 4 show the target-domain accuracy vs. number of epochs among ATDA, Co+ATDA, B-Net-1T and B-Net. Besides, we show the accuracy of ATDA trained with clean source data (ATDA-TCS) as a reference point. When accuracy of one method is close to that of ATDA-TCS (red dash line), this method successfully eliminates noise effects. From our observations, it is clear that B-Net

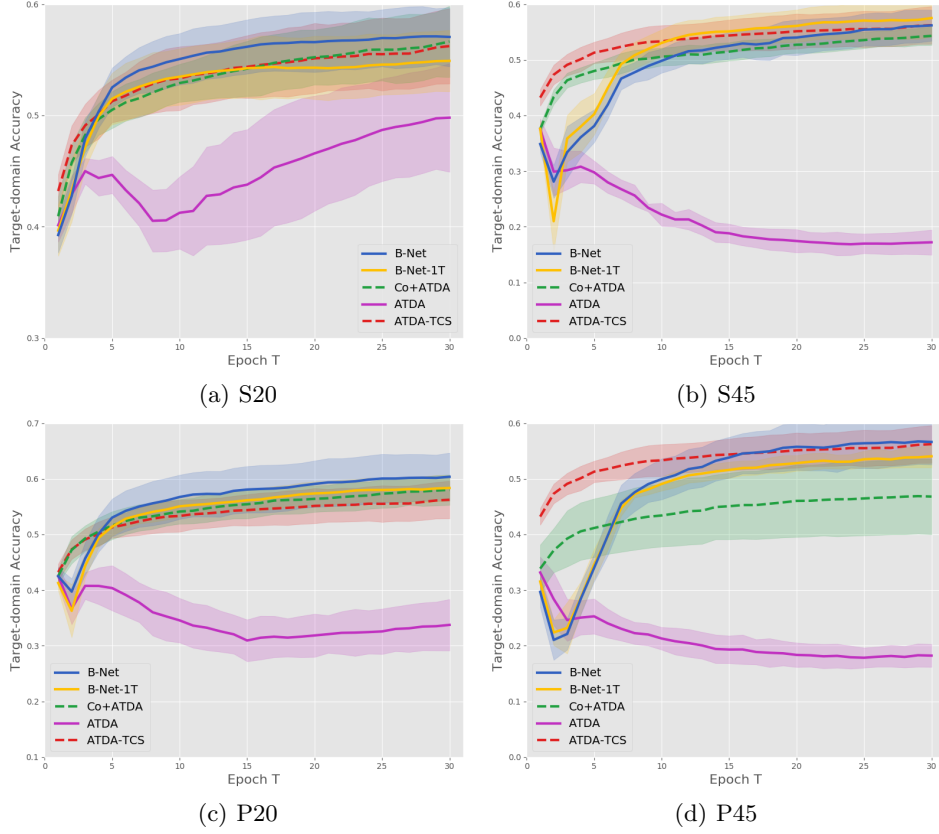


Fig. 4. Target-domain accuracy vs. number of epochs on four $MNIST \rightarrow SYND$ tasks.

Table 1. Target-domain accuracy on $SYND \leftrightarrow MNIST$ (8 tasks). Bold value represents highest accuracy in each row.

Tasks	Type	DAN	DANN	ATDA	TCL	Co+ATDA	B-Net-1T	B-Net
$S \rightarrow M$	P20	90.17%	79.06%	55.95%	80.81%	95.37%	93.45%	95.29%
	P45	67.00%	55.34%	53.66%	55.97%	75.43%	83.53%	90.21%
	S20	90.74%	75.19%	89.87%	80.23%	95.22%	94.44%	95.88%
	S45	89.31%	65.87%	87.53%	68.54%	92.03%	94.89%	94.97%
$M \rightarrow S$	P20	40.82%	58.78%	33.74%	58.88%	58.02%	58.35%	60.36%
	P45	28.41%	43.70%	19.50%	45.31%	46.80%	54.05%	56.62%
	S20	30.62%	53.52%	49.80%	56.74%	56.64%	54.90%	57.05%
	S45	28.21%	43.76%	17.20%	49.91%	54.29%	57.51%	56.18%
Average		58.16%	58.01%	50.91%	62.05%	71.73%	73.89%	75.82%

is very close to ATDA-TCS in 7 out of 8 tasks (except for $S \rightarrow M$ task with P45, Figure 3-(d)), which is an evidence of Theorem 3. Since P45 case is the hardest one, it is reasonable that B-Net cannot perfectly eliminate noise effects. An interesting phenomenon is that, B-Net outperforms ATDA-TCS in 2 $M \rightarrow S$ tasks (Figure 4-(a), (c)). This means that B-Net transfers more useful knowledge (from noisy source data to unlabeled target data) even than ATDA (from clean source data to unlabeled target data).

5.5 Results on real-world WUDA (including 3 tasks)

Finally, we show our results on real-world WUDA tasks. Table 2 reports the target-domain accuracy for 3 tasks. B-Net enjoys the best performance on all tasks. It should be noted that, in both $Bing \rightarrow Caltech256$ and $Bing \rightarrow ImageNet$ tasks, ATDA is slightly worse than B-Net. However, in

Bing→*SUN* task, ATDA is much worse than B-Net. The reason is that the DIR between *Bing* and *SUN* are more affected by noisy source data. This phenomenon is also observed when comparing DANN and TCL. Compared to Co+ATDA, ATDA is slightly better than Co+ATDA. This abnormal phenomenon can be explained using Eq. (4). In Eq. (4), after using Co-teaching to assign pseudo labels for noisy source data (\hat{P}_s in Figure 1), the second term in Δ'_s may increase, which results in $\Delta_p > \Delta$, i.e., noise effects actually increase. This phenomenon is an evidence that a two-step method may not really reduce noise effects.

Table 2. Target-domain accuracy on real-world tasks. The source domain is the *Bing* dataset that contains noisy information from the Internet. Bold value represents highest accuracy in each row.

Target	DAN	DANN	ATDA	TCL	Co+ATDA	B-Net-1T	B-Net
<i>Caltech256</i>	77.83%	78.00%	80.84%	79.35%	79.89%	81.26%	81.71%
<i>Imagenet</i>	70.29%	72.16%	74.89%	72.53%	74.73%	74.81%	75.00%
<i>SUN</i>	24.56%	26.80%	26.26%	28.80%	26.31%	30.45%	30.54%
Average	57.56%	58.99%	60.66%	60.23%	60.31%	62.17%	62.42%

6 Conclusions

This paper opens a new problem called *wildly unsupervised domain adaptation* (WUDA). However, existing UDA methods cannot handle WUDA well. Under the theoretical guidance, we propose a robust one-step approach called *Butterfly*. Butterfly maintains four deep networks simultaneously: Two take care of all adaptations; while the other two can focus on classification in target domain. We compare Butterfly with existing UDA methods on 32 simulated and 3 real-world WUDA tasks. Empirical results demonstrate that Butterfly can robustly transfer knowledge from noisy source data to unlabeled target data. In future, we can extend our Butterfly framework to address few-shot DA and open-set UDA when source domain contains noisy data.

References

1. D. Arpit, S. Jastrzebski, N. Ballas, D. Krueger, E. Bengio, M. Kanwal, T. Maharaj, A. Fischer, A. Courville, and Y. Bengio. A closer look at memorization in deep networks. In *ICML*, 2017.
2. S. Ben-David, J. Blitzer, K. Crammer, A. Kulesza, F. Pereira, and J. W. Vaughan. A theory of learning from different domains. *MLJ*, 79(1-2):151–175, 2010.
3. Y. Bengio. Evolving culture versus local minima. In *Growing Adaptive Machines*, pages 109–138. 2014.
4. A. Bergamo and L. Torresani. Exploiting weakly-labeled web images to improve object classification: a domain adaptation approach. In *NeurIPS*, pages 181–189, 2010.
5. J. Deng, W. Dong, R. Socher, L. Li, K. Li, and F. Li. Imagenet: A large-scale hierarchical image database. In *CVPR*, pages 248–255, 2009.
6. Y. Ganin and V. S. Lempitsky. Unsupervised domain adaptation by backpropagation. In *ICML*, pages 1180–1189, 2015.
7. Y. Ganin, E. Ustinova, H. Ajakan, P. Germain, H. Larochelle, F. Laviolette, M. Marchand, and V. S. Lempitsky. Domain-adversarial training of neural networks. *JMLR*, 17:59:1–59:35, 2016.
8. M. Ghifary, D. Balduzzi, W. B. Kleijn, and M. Zhang. Scatter component analysis : A unified framework for domain adaptation and domain generalization. *TPAMI*, 39(7):1414–1430, 2017.
9. B. Gong, Y. Shi, F. Sha, and K. Grauman. Geodesic flow kernel for unsupervised domain adaptation. In *CVPR*, pages 2066–2073, 2012.
10. M. Gong, K. Zhang, B. Huang, C. Glymour, D. Tao, and K. Batmanghelich. Causal generative domain adaptation networks. *CoRR*, abs/1804.04333, 2018.
11. M. Gong, K. Zhang, T. Liu, D. Tao, and C. Glymour. Domain adaptation with conditional transferable components. In *ICML*, pages 2839–2848, 2016.
12. A. Gretton, K. M. Borgwardt, M. J. Rasch, B. Schölkopf, and A. J. Smola. A kernel two-sample test. *JMLR*, 13:723–773, 2012.
13. G. Griffin, A. Holub, and P. Perona. Caltech-256 object category dataset. Technical report, California Institute of Technology, 2007.

14. Y. Guo and M. Xiao. Cross language text classification via subspace co-regularized multi-view learning. In *ICML*, 2012.
15. B. Han, Q. Yao, X. Yu, G. Niu, M. Xu, W. Hu, I. W. Tsang, and M. Sugiyama. Co-teaching: Robust training of deep neural networks with extremely noisy labels. In *NeurIPS*, pages 8527–8537, 2018.
16. J. Hoffman, E. Tzeng, T. Park, J. Zhu, P. Isola, K. Saenko, A. A. Efros, and T. Darrell. Cycada: Cycle-consistent adversarial domain adaptation. In *ICML*, pages 1994–2003, 2018.
17. L. Jiang, Z. Zhou, T. Leung, L. Li, and F. Li. Mentornet: Learning data-driven curriculum for very deep neural networks on corrupted labels. In *ICML*, pages 2309–2318, 2018.
18. J. Lee and M. Raginsky. Minimax statistical learning with wasserstein distances. In *NeurIPS*, pages 2692–2701, 2018.
19. K. Lee, X. He, L. Zhang, and L. Yang. Cleannet: Transfer learning for scalable image classifier training with label noise. In *CVPR*, pages 5447–5456, 2018.
20. Y. Li, X. Tian, M. Gong, Y. Liu, T. Liu, K. Zhang, and D. Tao. Deep domain generalization via conditional invariant adversarial networks. In *ECCV*, pages 647–663, 2018.
21. T. Liu and D. Tao. Classification with noisy labels by importance reweighting. *TPAMI*, 38(3):447–461, 2016.
22. M. Long, Y. Cao, J. Wang, and M. I. Jordan. Learning transferable features with deep adaptation networks. In *ICML*, pages 97–105, 2015.
23. E. Malach and S. Shalev-Shwartz. Decoupling "when to update" from "how to update". In *NeurIPS*, pages 961–971, 2017.
24. S. Motiian, Q. Jones, S. M. Iranmanesh, and G. Doretto. Few-shot adversarial domain adaptation. In *NeurIPS*, pages 6673–6683, 2017.
25. K. Saito, Y. Ushiku, and T. Harada. Asymmetric tri-training for unsupervised domain adaptation. In *ICML*, pages 2988–2997, 2017.
26. K. Saito, K. Watanabe, Y. Ushiku, and T. Harada. Maximum classifier discrepancy for unsupervised domain adaptation. In *CVPR*, pages 3723–3732, 2018.
27. F. Schroff, A. Criminisi, and A. Zisserman. Harvesting image databases from the web. *TPAMI*, 33(4):754–766, 2011.
28. Y. Shu, Z. Cao, M. Long, and J. Wang. Transferable curriculum for weakly-supervised domain adaptation. In *AAAI*, 2019.
29. T. Tommasi and T. Tuytelaars. A testbed for cross-dataset analysis. In *ECCV TASK-CV Workshops*, pages 18–31, 2014.
30. E. Tzeng, J. Hoffman, T. Darrell, and K. Saenko. Simultaneous deep transfer across domains and tasks. In *ICCV*, pages 4068–4076, 2015.
31. E. Tzeng, J. Hoffman, K. Saenko, and T. Darrell. Adversarial discriminative domain adaptation. In *CVPR*, pages 2962–2971, 2017.
32. J. Xiao, J. Hays, K. A. Ehinger, A. Oliva, and A. Torralba. SUN database: Large-scale scene recognition from abbey to zoo. In *CVPR*, pages 3485–3492, 2010.
33. M. Xiao and Y. Guo. Feature space independent semi-supervised domain adaptation via kernel matching. *TPAMI*, 37(1):54–66, 2015.
34. T. Xiao, T. Xia, Y. Yang, C. Huang, and X. Wang. Learning from massive noisy labeled data for image classification. In *CVPR*, pages 2691–2699, 2015.
35. K. Zhang, M. Gong, and B. Schölkopf. Multi-source domain adaptation: A causal view. In *AAAI*, pages 3150–3157, 2015.
36. K. Zhang, B. Schölkopf, K. Muandet, and Z. Wang. Domain adaptation under target and conditional shift. In *ICML*, pages 819–827, 2013.

A Review of generation of noisy labels

This section presents a review on two label-noise generation processes.

A.1 Transition matrix

We assume that there is a clean multivariate random variable (X_s, Y_s) defined on $\mathcal{X} \times \mathcal{Y}$ with a probability density $p_s(x_s, y_s)$, where $\mathcal{Y} = \{1, \dots, K\}$ is a label set with K labels. However, samples of (X_s, Y_s) cannot be directly obtained and we only can observe noisy source data from the multivariate random variable (X_s, \tilde{Y}_s) defined on $\mathcal{X} \times \mathcal{Y}$ with a probability density $\tilde{p}_s(x_s, \tilde{y}_s)$. $\tilde{p}_s(x_s, \tilde{y}_s)$ is generated by a transition probability $\Pr(\tilde{Y}_s = j | Y_s = i)$, i.e., the flip rate from a clean label i to a noisy label j . When we generate $\tilde{p}_s(x_s, \tilde{y}_s)$ using Q , we often assume that $\sum_{y_s=1}^K p_s(x_s, y_s) = \sum_{\tilde{y}_s=1}^K \tilde{p}_s(x_s, \tilde{y}_s)$, i.e., the class conditional noise [21]. All these transition probabilities are summarized into a transition matrix Q , where $Q_{ij} = \Pr(\tilde{Y}_s = j | Y_s = i)$.

The transition matrix Q is easily estimated in certain situations [21]. However, in more complex situations, such as clothing1M dataset [34], noisy source data is directly generated by selecting data from a pool, which mixes correct data (data with correct labels) and incorrect data (data with incorrect labels). Namely, how the correct label i is corrupted to j ($i \neq j$) is unclear.

A.2 Sample selection

Formally, there is a multivariate random variable (X_s, Y_s, V_s) defined on $\mathcal{X} \times \mathcal{Y} \times \mathcal{V}$ with a probability density $p_s^{\text{po}}(x_s, y_s, v_s)$, where $\mathcal{V} = \{0, 1\}$ and $V_s = 1$ means “correct” and $V_s = 0$ means “incorrect”. Nonetheless, samples from (X_s, Y_s, V_s) cannot be obtained and we can only observe (X_s, \tilde{Y}_s) from a distribution with the following density.

$$\tilde{p}_s(x_s, \tilde{y}_s) = \sum_{v_s=0}^1 p_{X_s, Y_s | V_s}^{\text{po}}(x_s, y_s | v_s) p_{V_s}^{\text{po}}(v_s), \quad (8)$$

where $p_{V_s}^{\text{po}}(v_s) = \int_{\mathcal{X}} \sum_{y_s=1}^K p_s^{\text{po}}(x_s, y_s, v_s) dx_s$. The density in Eq. (8) means that we lost the information from V_s . If we uniformly select samples drawn from $\tilde{p}_s(x_s, \tilde{y}_s)$, the noisy rate of these samples is $p_{V_s}^{\text{po}}(0)$. It is clear that the multivariate random variable $(X_s, Y_s | V_s = 1)$ is the clean multivariate random variable (X_s, Y_s) defined in Appendix A.1. Then, $q_s(x_s, y_s)$ is used to describe the density of incorrect multivariate random variable $(X_s, Y_s | V_s = 0)$. Using $p_s(x_s, y_s)$ and $q_s(x_s, y_s)$, $\tilde{p}_s(x_s, \tilde{y}_s)$ can be expressed by the following equation.

$$\tilde{p}_s(x_s, \tilde{y}_s) = (1 - \rho)p_s(x_s, y_s) + \rho q_s(x_s, y_s), \quad (9)$$

where $\rho = p_{V_s}^{\text{po}}(0)$. Here, we do not assume $\sum_{y_s=1}^K p_s(x_s, y_s) = \sum_{y_s=1}^K q_s(x_s, y_s)$. To reduce noise effects from incorrect data, scholars aim to recover the information of V_s , i.e., to select correct data from data drawn from $\tilde{p}_s(x_s, \tilde{y}_s)$ [15, 17, 23].

B Transition matrix Q

Precise definitions of Symmetry flipping and Pair flipping are presented below, where ρ is the noisy rate and K is the number of labels.

$$\begin{aligned} \text{Symmetry flipping: } Q &= \begin{bmatrix} 1 - \rho & \frac{\rho}{K-1} & \dots & \frac{\rho}{K-1} & \frac{\rho}{K-1} \\ \frac{\rho}{K-1} & 1 - \rho & \frac{\rho}{K-1} & \dots & \frac{\rho}{K-1} \\ \vdots & & \ddots & & \vdots \\ \frac{\rho}{K-1} & \dots & \frac{\rho}{K-1} & 1 - \rho & \frac{\rho}{K-1} \\ \frac{\rho}{K-1} & \frac{\rho}{K-1} & \dots & \frac{\rho}{K-1} & 1 - \rho \end{bmatrix}, \\ \text{Pair flipping: } Q &= \begin{bmatrix} 1 - \rho & \rho & 0 & \dots & 0 \\ 0 & 1 - \rho & \rho & & 0 \\ \vdots & & \ddots & \ddots & \vdots \\ 0 & & & 1 - \rho & \rho \\ \rho & 0 & \dots & 0 & 1 - \rho \end{bmatrix}. \end{aligned}$$

C Results on Amazon products reviews

Tables 3 and 4 report the target-domain accuracy of each method for 24 human-sentiment tasks. For these tasks, B-Net has the highest average accuracy. It should be noted that two-step method does not always work, such as for 20%-noise situation. The main reason is Co-teaching performs poorly when pinpointing clean source data from noisy source data. Another observation is that noise effects are not eliminated like classification results on $SYND \leftrightarrow MNIST$. The main reason is that these datasets provide fixed features and we cannot extract better features in the training process. However, in $SYND \leftrightarrow MNIST$ tasks, we can gradually obtain better features for each domain and finally eliminate noise effects.

Table 3. Target-domain accuracy on 12 *human-sentiment* tasks with 20% noisy rate. Bold values mean highest values in each row.

Tasks	DAN	DANN	ATDA	TCL	Co+ATDA	B-Net-1T	B-Net
$B \rightarrow D$	68.28%	68.08%	70.31%	71.40%	66.70%	72.42%	71.84%
$B \rightarrow E$	63.78%	63.53%	72.79%	65.08%	68.89%	73.50%	75.92%
$B \rightarrow K$	65.48%	64.63%	71.79%	66.80%	66.51%	74.63%	76.32%
$D \rightarrow B$	64.63%	64.52%	70.25%	67.33%	68.04%	70.69%	70.56%
$D \rightarrow E$	65.33%	65.16%	69.99%	66.74%	67.32%	72.74%	73.73%
$D \rightarrow K$	65.68%	66.28%	74.53%	68.82%	72.20%	76.47%	77.97%
$E \rightarrow B$	60.41%	60.15%	63.89%	63.13%	61.08%	65.52%	62.22%
$E \rightarrow D$	62.35%	61.67%	62.30%	62.93%	59.77%	64.22%	63.53%
$E \rightarrow K$	72.05%	71.51%	74.00%	75.36%	70.85%	75.80%	78.96%
$K \rightarrow B$	59.94%	59.40%	63.53%	62.77%	61.22%	64.16%	63.36%
$K \rightarrow D$	61.46%	61.51%	64.66%	64.16%	64.94%	67.52%	66.98%
$K \rightarrow E$	70.60%	72.23%	74.75%	74.14%	69.69%	75.21%	76.96%
Average	65.00%	64.89%	69.40%	67.39%	66.43%	71.07%	71.53%

Table 4. Target-domain accuracy on 12 *human-sentiment* tasks with 45% noisy rate. Bold values mean highest values in each row.

Tasks	DAN	DANN	ATDA	TCL	Co+ATDA	B-Net-1T	B-Net
$B \rightarrow D$	52.43%	52.98%	53.56%	54.44%	54.32%	54.89%	56.59%
$B \rightarrow E$	52.17%	53.50%	55.14%	54.14%	57.34%	56.93%	55.74%
$B \rightarrow K$	52.89%	51.84%	51.14%	53.32%	53.28%	58.38%	57.00%
$D \rightarrow B$	53.11%	53.04%	54.48%	53.27%	55.95%	51.37%	55.15%
$D \rightarrow E$	51.30%	53.04%	54.21%	53.77%	56.08%	55.04%	58.91%
$D \rightarrow K$	52.15%	53.17%	57.99%	52.45%	59.94%	58.43%	66.20%
$E \rightarrow B$	51.38%	51.08%	52.54%	52.14%	53.30%	50.53%	54.93%
$E \rightarrow D$	52.83%	51.24%	49.02%	52.57%	49.62%	50.11%	52.88%
$E \rightarrow K$	54.21%	53.58%	51.66%	55.04%	52.10%	48.62%	56.12%
$K \rightarrow B$	50.44%	51.77%	51.96%	51.50%	52.59%	49.88%	51.39%
$K \rightarrow D$	52.20%	51.45%	52.86%	53.19%	54.52%	52.91%	53.53%
$K \rightarrow E$	54.72%	53.33%	52.11%	53.46%	52.62%	53.11%	53.71%
Average	52.49%	52.50%	53.65%	53.06%	54.31%	53.35%	56.01%

D Experimental settings

D.1 Network structure and optimizer

We implement all methods on Python 3.6 with a NVIDIA P100 GPU. We use MomentumSGD for optimization in digit and real-world tasks, and set the momentum as 0.9. We use Adagrad for

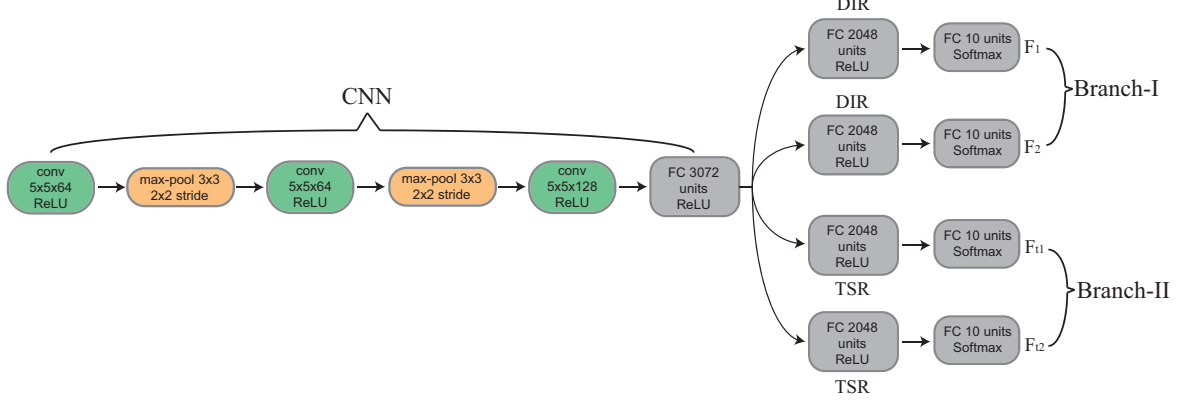


Fig. 5. The architecture of B-Net for tasks $SYND \leftrightarrow MNIST$. We added BN layer in the last convolution layer in CNN and FC layers in F_1 and F_2 . We also used dropout in the last convolution layer in CNN and FC layers in F_1 , F_2 , F_{t1} and F_{t2} (dropout probability is set to 0.5).

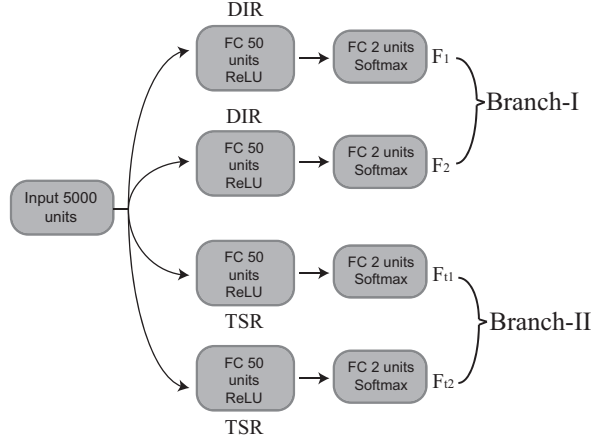


Fig. 6. The architecture of B-Net for tasks *human-sentiment analysis*. We added BN layer in the first FC layers in F_1 and F_2 . We also used dropout in the first FC layers in F_1 , F_2 , F_{t1} and F_{t2} (dropout probability is set to 0.5).

optimization in human-sentiment tasks because of sparsity of review data [25]. F_1 , F_2 , F_{t1} and F_{t2} are 6-layer CNN (3 convolutional layers and 3 fully-connected layers) for digit tasks; and are 3-layer neural networks (3 fully-connected layers) for human-sentiment tasks; and are 4-layer neural networks (4 fully-connected layers) for real-world tasks. The ReLU active function is used as activation function of these networks. Besides, dropout and batch normalization are also used. The network topology is shown in Figures 5, 6, 7. As deep networks are highly nonconvex, even with the same network and optimization method, different initializations can lead to different local optimal. Thus, following [15,23], we also take four networks with the same architecture but different initializations as four classifiers.

D.2 Experimental setup

For all 35 WUDA tasks, T_k is set to 5, T_{max} is set to 30. Learning rate is set to 0.01 for simulated tasks and 0.05 for real-world tasks, γ_t is set to 0.05 for simulated tasks and 0.02 for real-world tasks. Confidence level of labelling function in line 8 of Algorithm 2 is set to 0.95 for 8 digit tasks, and 0.9 for 24 human-sentiment tasks and 0.8 for 3 real-world tasks. γ is set to 0.4 for digit tasks, 0.1 for human-sentiment tasks and 0.2 for real-world tasks. $n_{t,max}^l$ is set to 15,000 for digit tasks, 500 for human-sentiment tasks and 4000 for real-world tasks. N_{max} is set to 1000 for digit tasks and 200 for

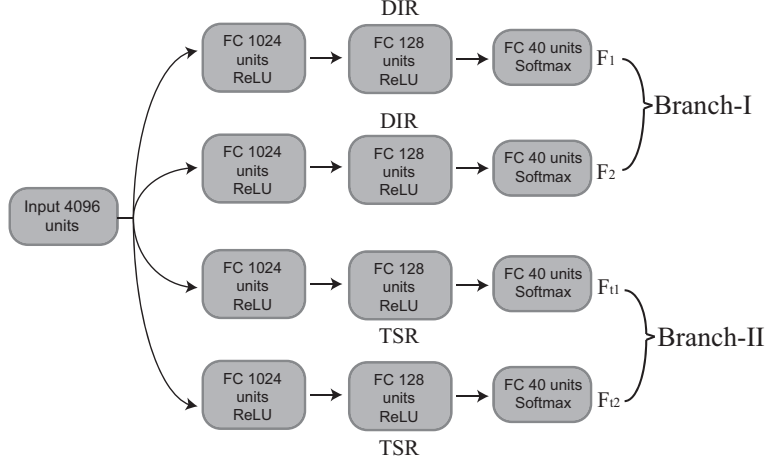


Fig. 7. The architecture of B-Net for tasks $SYND \leftrightarrow MNIST$. We added BN layer in the first FC layers in F_1 , F_2 , F_{t1} and F_{t2} . We also used dropout in the first FC layers in F_1 , F_2 , F_{t1} and F_{t2} (dropout probability is set to 0.5).

human-sentiment and real-world tasks. Batch size is set to 128 for digit and real-world tasks and 24 for human-sentiment tasks. Penalty parameter is set to 0.01 for digit and real-world tasks and 0.001 for human-sentiment tasks.

To fairly compare all methods, they have the same network structure. Namely, ATDA, DAN, DANN, TCL, B-Net-1T and B-Net adopt the same network structure for each dataset. Note that DANN and TCL use the same structure for their discriminate networks. All experiments are repeated ten times and we report the average accuracy value and STD of accuracy values of ten experiments.

D.3 Links to datasets

We give following links to download datasets used in this paper.

MNIST and *SYN Digit (SYND)* can be downloaded from official code of ATDA. The link is <https://github.com/ksaito-ut/atda>.

Amazon product reviews can be downloaded from the official code of marginalized Stacked Denoising Autoencoder (mSDA). The link is <https://www.cse.wustl.edu/~mchen/code/mSDA.tar>.

BCIS datasets can be downloaded from the website of the project “A Testbed for Cross-Dataset Analysis”: <https://sites.google.com/site/crossdataset/home/files> (“setup DENSE decaf7”, 1.3GB, decaf7 features).

E Datasets visualization

Figure 8 shows datasets: *SYND* and *MNIST*. Figure 9 shows datasets: *Bing*, *Caltech256*, *Imagenet* and *SUN* (taking “horse” as the common class).

F Additional experiments

To show how accuracy changes when the noisy rate increases, we also test target-domain accuracy of each method when noisy rate changes from 10% to 60% in task $SYND \rightarrow MNIST$, where the noisy type is Symmetry-flipping. Figure 10 shows the target-domain accuracy vs. noisy rate. It is clear that B-Net is more robust than other baselines across the whole range of noise rates (i.e., 10%-60%).

G Running time

Table 5 shows the average running time of each method on the task $SYND \rightarrow MNIST$. Although B-Net trains four networks, its running time is still comparable to most baselines.

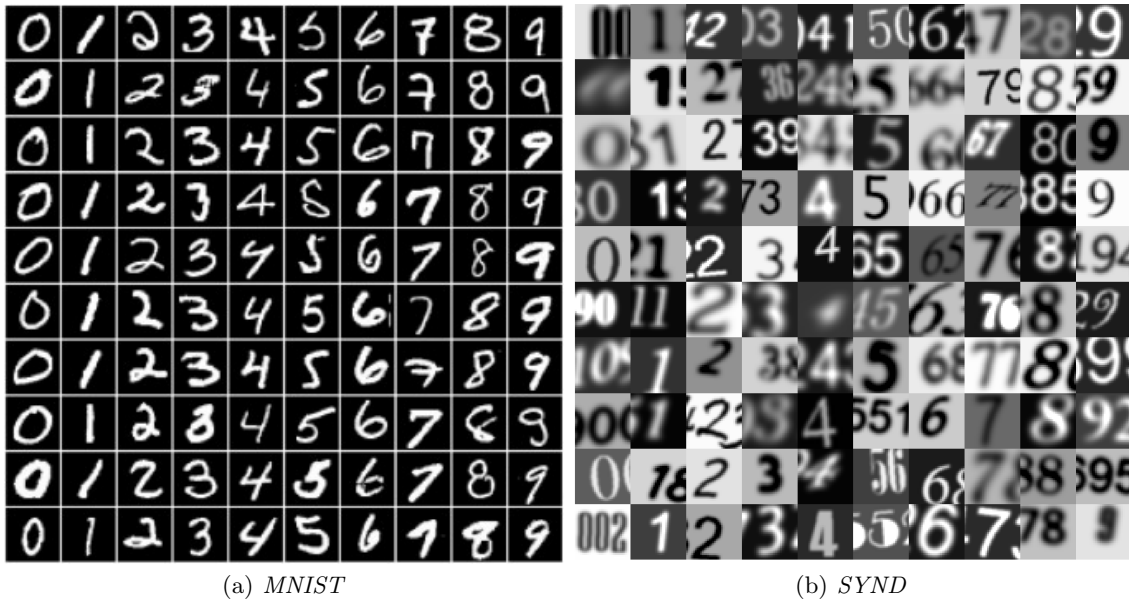


Fig. 8. Visualization of *MNIST* and *SYND*.

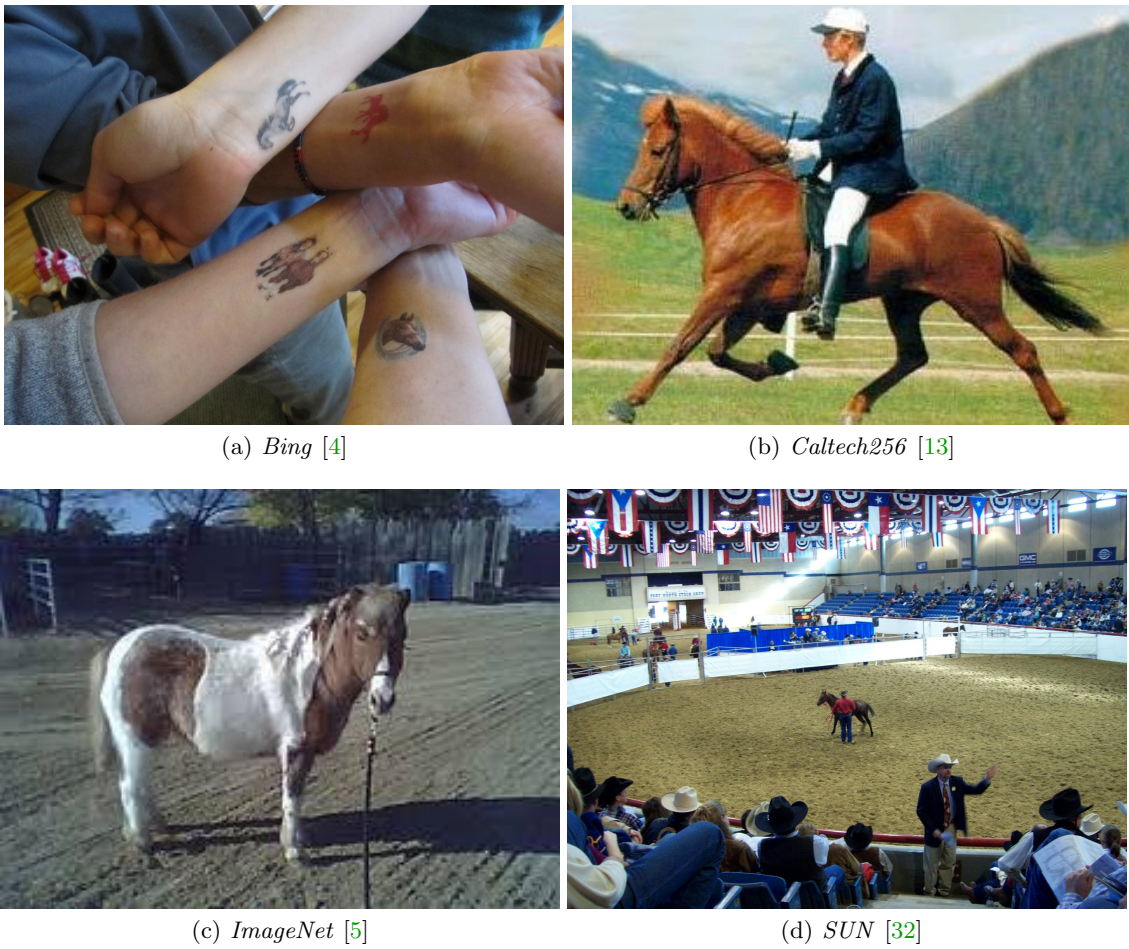


Fig. 9. Visualization of *Bing*, *Caltech256*, *ImageNet* and *SUN* (taking “horse” as the common class).

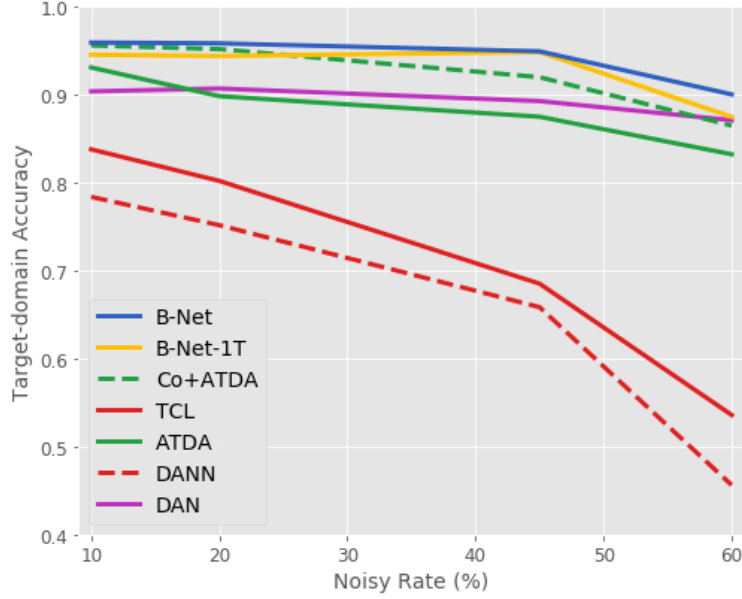


Fig. 10. Target-domain accuracy vs. noisy rate (%) in task $SYND \rightarrow MNIST$.

Table 5. Running time for each method on the task $SYND \rightarrow MNIST$ (minutes).

Methods	DAN	DANN	ATDA	TCL	Co+ATDA	B-Net-1T	B-Net
Time	17.17	9.02	17.17	14.04	18.28	17.08	20.55

H Proofs

This section presents proofs of our theorems.

H.1 Proof of Theorem 1

Proof. We will first prove Eq. (1) (Case 1) and then prove Eq. (2) (Case 2).

Case 1. According to definition of $\tilde{R}_s(h)$, we have

$$\begin{aligned}
 \tilde{R}_s(h) &= \mathbb{E}_{\tilde{p}_s(x_s, \tilde{y}_s)}[\ell(h(x_s), \tilde{y}_s)] \\
 &= \int_{\mathcal{X}} \sum_{\tilde{y}_s=1}^K \ell(h(x_s), \tilde{y}_s) \tilde{p}_s(x_s, \tilde{y}_s) dx_s \\
 &= \int_{\mathcal{X}} \sum_{\tilde{y}_s=1}^K \ell(h(x_s), \tilde{y}_s) \tilde{p}_{\tilde{Y}_s|X_s}(\tilde{y}_s|x_s) p_{x_s}(x_s) dx_s \\
 &= \int_{\mathcal{X}} \tilde{\boldsymbol{\eta}}^T(x_s) \boldsymbol{\ell}(h(x_s)) p_{x_s}(x_s) dx_s,
 \end{aligned} \tag{10}$$

where $\boldsymbol{\ell}(h(x_s)) = [\ell(h(x_s), 1), \dots, \ell(h(x_s), K)]^T$ and $\tilde{\boldsymbol{\eta}}(x_s) = [\tilde{p}_{\tilde{Y}_s|X_s}(1|x_s), \dots, \tilde{p}_{\tilde{Y}_s|X_s}(K|x_s)]^T$. According to definition of the transition matrix Q , we know that

$$\tilde{\boldsymbol{\eta}}^T(x_s) = \boldsymbol{\eta}^T(x_s) Q, \tag{11}$$

where $\boldsymbol{\eta}(x_s) = [p_{Y_s|X_s}(1|x_s), \dots, p_{Y_s|X_s}(K|x_s)]^T$. Substituting Eq. (11) into Eq. (10), we have

$$\begin{aligned}\tilde{R}_s(h) &= \int_{\mathcal{X}} \boldsymbol{\eta}^T(x_s) Q \boldsymbol{\ell}(h(x_s)) p_{x_s}(x_s) dx_s \\ &= \int_{\mathcal{X}} \boldsymbol{\eta}^T(x_s) I \boldsymbol{\ell}(h(x_s)) p_{x_s}(x_s) dx_s + \int_{\mathcal{X}} \boldsymbol{\eta}^T(x_s) (Q - I) \boldsymbol{\ell}(h(x_s)) p_{x_s}(x_s) dx_s \\ &= R_s(h) + \mathbb{E}_{p_{x_s}(x_s)} [\boldsymbol{\eta}^T(x_s) (Q - I) \boldsymbol{\ell}(h(x_s))].\end{aligned}$$

Hence, Case 1 is proved.

Case 2. According to definition of $\tilde{R}_s(h)$ and Eq. (9), we have

$$\begin{aligned}\tilde{R}_s(h) &= \mathbb{E}_{\tilde{p}_s(x_s, \tilde{y}_s)} [\boldsymbol{\ell}(h(x_s), \tilde{y}_s)] \\ &= \int_{\mathcal{X}} \sum_{\tilde{y}_s=1}^K \boldsymbol{\ell}(h(x_s), \tilde{y}_s) \tilde{p}_s(x_s, \tilde{y}_s) dx_s \\ &= \int_{\mathcal{X}} \sum_{y_s=1}^K \boldsymbol{\ell}(h(x_s), y_s) ((1 - \rho) p_s(x_s, y_s) + \rho q_s(x_s, y_s)) dx_s \\ &= (1 - \rho) \int_{\mathcal{X}} \sum_{y_s=1}^K \boldsymbol{\ell}(h(x_s), y_s) p_s(x_s, y_s) dx_s + \rho \int_{\mathcal{X}} \sum_{y_s=1}^K \boldsymbol{\ell}(h(x_s), y_s) q_s(x_s, y_s) dx_s \\ &= (1 - \rho) R_s(h) + \rho \int_{\mathcal{X}} \sum_{y_s=1}^K \boldsymbol{\ell}(h(x_s), y_s) q_{Y_s|X_s}(y_s|x_s) q_{x_s}(x_s) dx_s.\end{aligned}\tag{12}$$

Let $\boldsymbol{\eta}_q(x_s) = [q_{Y_s|X_s}(1|x_s), \dots, q_{Y_s|X_s}(K|x_s)]^T$, we have

$$\tilde{R}_s(h) = (1 - \rho) R_s(h) + \rho \mathbb{E}_{q_{x_s}(x_s)} [\boldsymbol{\eta}_q^T(x_s) \boldsymbol{\ell}(h(x_s))].$$

Hence, Case 2 is proved.

H.2 Proof of Theorem 2

Proof. For any labelling function h , we have

$$\begin{aligned}R_t(h, f_t) &= R_t(h, f_t) + \tilde{R}_s(h) - \tilde{R}_s(h) + R_s(h, f_t) - R_s(h, f_t) \\ &= \tilde{R}_s(h) + R_t(h, f_t) - \tilde{R}_s(h, f_t) + R_s(h, f_t) - R_s(h) + R_s(h) - \tilde{R}_s(h) \\ &\quad + \tilde{R}_s(h, f_t) - R_s(h, f_t).\end{aligned}\tag{13}$$

Since we do not know f_t , we substitute following equations into Eq. (13),

$$\begin{aligned}R_t(h, f_t) &= R_t(h, \tilde{f}_t) + R_t(h, f_t) - R_t(h, \tilde{f}_t), \\ \tilde{R}_s(h, f_t) &= \tilde{R}_s(h, \tilde{f}_t) + \tilde{R}_s(h, f_t) - \tilde{R}_s(h, \tilde{f}_t), \\ R_s(h, f_t) &= R_s(h, \tilde{f}_t) + R_s(h, f_t) - R_s(h, \tilde{f}_t).\end{aligned}$$

Then, we have

$$\begin{aligned}R_t(h, f_t) &= \tilde{R}_s(h) + R_t(h, \tilde{f}_t) - \tilde{R}_s(h, \tilde{f}_t) + R_s(h, \tilde{f}_t) - R_s(h) \\ &\quad + R_s(h) - \tilde{R}_s(h) + \tilde{R}_s(h, \tilde{f}_t) - R_s(h, \tilde{f}_t) + R_t(h, f_t) - R_t(h, \tilde{f}_t) \\ &\leq \tilde{R}_s(h) + |R_t(h, \tilde{f}_t) - \tilde{R}_s(h, \tilde{f}_t)| + |R_s(h, \tilde{f}_t) - R_s(h)| \\ &\quad + |\tilde{R}_s(h) - R_s(h)| + |\tilde{R}_s(h, \tilde{f}_t) - R_s(h, \tilde{f}_t)| + |R_t(h, f_t) - R_t(h, \tilde{f}_t)|.\end{aligned}$$

Hence, this theorem is proved.

H.3 Proof of Theorem 3

Preliminary Before stating the proof, we first present a random variable below.

Let (X_t, V_t) be a m.r.v. defined on $\mathcal{X} \times \mathcal{V}$ with respective a density $p_t^{\text{po}}(x_t, v_t)$, where $\mathcal{V} = \{0, 1\}$. V_t can be regarded as *perfect-selection random variables*. Namely, $V_t = 1$ means $f_t(x_t) = \tilde{f}_t(x_t)$ and $V_t = 0$ means $f_t(x_t) \neq \tilde{f}_t(x_t)$. Let $p_{V_t}^{\text{po}}(v_t)$ be the marginal density of $p_t^{\text{po}}(x_t, v_t)$. It is clear that, higher value of $p_{V_t}^{\text{po}}(V_t = 1)$ means that \tilde{f}_t is more like f_t . In following, we use $1 - \rho_{v_t}$ to represent $p_{V_t}^{\text{po}}(V_t = 1)$.

Then, we will show 1) relation between (X_s, Y_s, V_s) and (X_s, Y_s, U_s) , 2) relation between (X_t, V_t) and (X_t, U_t) and definitions of ρ_{01}^s and ρ_{01}^t . Based on (X_t, V_t) and (X_s, Y_s, V_s) defined in Appendix A.2, the densities of (X_s, Y_s, U_s) and (X_t, U_t) can be expressed as follows.

$$\begin{aligned} \tilde{p}_{X_s, Y_s | U_s}^{\text{po}}(x_s, y_s | i) &= \rho_{0i}^s p_{X_s, Y_s | V_s}^{\text{po}}(x_s, y_s | 0) + \rho_{1i}^s p_{X_s, Y_s | V_s}^{\text{po}}(x_s, y_s | 1), \\ \tilde{p}_{X_t | U_t}^{\text{po}}(x_t | i) &= \rho_{0i}^t p_{X_t | V_t}^{\text{po}}(x_t | 0) + \rho_{1i}^t p_{X_t | V_t}^{\text{po}}(x_t | 1), \end{aligned}$$

where $\rho_{ji}^s = \Pr(V_s = j | U_s = i)$ represents the probability of the event: $V_s = j$ given $U_s = i$, $\rho_{ji}^t = \Pr(V_t = j | U_t = i)$ represents the probability of the event: $V_t = j$ given $U_t = i$ ($i, j = 0, 1$). Since $p_s(x_s, y_s) = p_{X_s, Y_s | V_s}^{\text{po}}(x_s, y_s | 1)$, $q_s(x_s, y_s) = p_{X_s, Y_s | V_s}^{\text{po}}(x_s, y_s | 0)$, $p_{X_t | V_t}^{\text{po}}(x_t | 0) = p_{x_t}(x_t)1_A(x_t)/P_{x_t}(A) = q_{x_t}(x_t)$ and $p_{X_t | V_t}^{\text{po}}(x_t | 1) = p_{x_t}(x_t)1_B(x_t)/P_{x_t}(B) = p'_{x_t}(x_t)$ ($A = \{x : \tilde{f}_t(x) \neq f_t(x)\}$, $B = \mathcal{X}/A$), we have

$$\tilde{p}_{X_s, Y_s | U_s}^{\text{po}}(x_s, y_s | i) = \rho_{0i}^s q_s(x_s, y_s) + \rho_{1i}^s p_s(x_s, y_s), \quad (14)$$

$$\tilde{p}_{X_t | U_t}^{\text{po}}(x_t | i) = \rho_{0i}^t q_{x_t}(x_t) + \rho_{1i}^t p'_{x_t}(x_t). \quad (15)$$

Next, we give a lemma to show relation between $\tilde{R}_s^{\text{po}}(h, u_s)$ and $R_s(h)$.

Lemma 1 *Given the multivariate random variable (X_s, Y_s, U_s) with the probability $\tilde{p}_s^{\text{po}}(x_s, y_s, u_s)$ and Eq. (14), we have*

$$|\tilde{R}_s^{\text{po}}(h, u_s) - R_s(h)| \leq \rho_{01}^s \max\{\mathbb{E}_{q_s(x_s, y_s)}[\ell(h(x_s), y_s)], R_s(h)\}. \quad (16)$$

Proof. According to definition of $\tilde{R}_s^{\text{po}}(h, u_s)$ in Theorem 3, we have

$$\begin{aligned} \tilde{R}_s^{\text{po}}(h, u_s) &= (1 - \rho_{u_s})^{-1} \int_{\mathcal{X}} \sum_{u_s=0}^1 \sum_{y_s=1}^K u_s \ell(h(x_s), y_s) \tilde{p}_s^{\text{po}}(x_s, y_s, u_s) dx_s \\ &= (1 - \rho_{u_s})^{-1} \int_{\mathcal{X}} \sum_{y_s=1}^K \ell(h(x_s), y_s) \tilde{p}_{X_s, Y_s | U_s}^{\text{po}}(x_s, y_s | 1) \tilde{p}_{U_s}^{\text{po}}(1) dx_s \\ &\stackrel{(a)}{=} (1 - \rho_{u_s})^{-1} (1 - \rho_{u_s}) \int_{\mathcal{X}} \sum_{y_s=1}^K \ell(h(x_s), y_s) (\rho_{01}^s q_s(x_s, y_s) + \rho_{11}^s p_s(x_s, y_s)) dx_s \\ &= \rho_{01}^s \mathbb{E}_{q_s(x_s, y_s)}[\ell(h(x_s), y_s)] + \rho_{11}^s R_s(h), \end{aligned}$$

where (a) is based on the definition of ρ_{u_s} and Eq. (14). Thus, we have

$$\begin{aligned} |\tilde{R}_s^{\text{po}}(h, u_s) - R_s(h)| &= |\rho_{01}^s \mathbb{E}_{q_s(x_s, y_s)}[\ell(h(x_s), y_s)] - (1 - \rho_{11}^s) R_s(h)| \\ &\leq \rho_{01}^s \max\{\mathbb{E}_{q_s(x_s, y_s)}[\ell(h(x_s), y_s)], R_s(h)\}. \end{aligned}$$

This lemma is proved.

Similar with Lemma 1, we can obtain

$$|\tilde{R}_s^{\text{po}}(h, \tilde{f}_t, u_t) - R_s(h, \tilde{f}_t)| \leq \rho_{01}^s \max\{\mathbb{E}_{q_{x_s}(x_s)}[\ell(h(x_s), \tilde{f}_t(x_s))], R_s(h, \tilde{f}_t)\}. \quad (17)$$

Then, we give another lemma to show relation between $\tilde{R}_t^{\text{po}}(h, \tilde{f}_t, u_s)$ and $R_t(h, \tilde{f}_t)$.

Lemma 2 Given the multivariate random variable (X_t, U_t) with the probability $\tilde{p}_s^{\text{po}}(x_t, u_t)$ and Eq. (15), if $\mathbb{E}_{p'_{x_t}(x_t)}[\ell(h(x_t), f_t(x_t))] \leq R_t(h, f_t) + \rho_{01}^s M_t$, then we have

$$|\tilde{R}_t^{\text{po}}(h, \tilde{f}_t, u_t) - R_t(h, f_t)| \leq \rho_{01}^t \max\{\mathbb{E}_{q_{x_t}(x_t)}[\ell(h(x_t), \tilde{f}_t(x_t))], R_t(h, f_t)\} + \rho_{11}^t \rho_{01}^s M_t. \quad (18)$$

Proof. According to definition of $\tilde{R}_t^{\text{po}}(h, \tilde{f}_t, u_t)$ in Theorem 3, we have

$$\begin{aligned} \tilde{R}_t^{\text{po}}(h, \tilde{f}_t, u_t) &= (1 - \rho_{u_t})^{-1} \int_{\mathcal{X}} \sum_{u_t=0}^1 u_t \ell(h(x_t), \tilde{f}_t(x_t)) \tilde{p}_t^{\text{po}}(x_t, u_t) dx_t \\ &= (1 - \rho_{u_t})^{-1} \int_{\mathcal{X}} \ell(h(x_t), \tilde{f}_t(x_t)) \tilde{p}_{X_t|U_t}^{\text{po}}(x_t|1) \tilde{p}_{U_t}^{\text{po}}(1) dx_t \\ &\stackrel{(a)}{=} (1 - \rho_{u_t})^{-1} (1 - \rho_{u_t}) \int_{\mathcal{X}} \ell(h(x_s), \tilde{f}_t(x_t)) (\rho_{01}^t q_{x_t}(x_t) + \rho_{11}^t p_{X_t|V_t}^{\text{po}}(x_t|1)) dx_t \\ &= \rho_{01}^t \mathbb{E}_{q_{x_t}(x_t)}[\ell(h(x_t), \tilde{f}_t(x_t))] + \rho_{11}^t \int_{\mathcal{X}} \ell(h(x_t), \tilde{f}_t(x_t)) p_{X_t|V_t}^{\text{po}}(x_t|V_t = 1) dx_t \\ &\stackrel{(b)}{=} \rho_{01}^t \mathbb{E}_{q_{x_t}(x_t)}[\ell(h(x_t), \tilde{f}_t(x_t))] + \rho_{11}^t \int_{\mathcal{X}} \ell(h(x_t), f_t(x_t)) p_{X_t|V_t}^{\text{po}}(x_t|V_t = 1) dx_t \\ &= \rho_{01}^t \mathbb{E}_{q_{x_t}(x_t)}[\ell(h(x_t), \tilde{f}_t(x_t))] + \rho_{11}^t \int_{\mathcal{X}} \ell(h(x_t), f_t(x_t)) p'_{x_t}(x_t) dx_t \\ &= \rho_{01}^t \mathbb{E}_{q_{x_t}(x_t)}[\ell(h(x_t), \tilde{f}_t(x_t))] + \rho_{11}^t \mathbb{E}_{p'_{x_t}(x_t)}[\ell(h(x_t), f_t(x_t))], \end{aligned} \quad (19)$$

where (a) is based on the definition of ρ_{u_s} and Eq. (14) and (b) is based on the definition of V_t ($f_t(x_t) = \tilde{f}_t(x_t)$ when $V_t = 1$). Since $\mathbb{E}_{p'_{x_t}(x_t)}[\ell(h(x_t), f_t(x_t))] \leq R_t(h, f_t) + \rho_{01}^s M_t$, we have

$$\tilde{R}_t^{\text{po}}(h, \tilde{f}_t, u_t) \leq \rho_{01}^t \mathbb{E}_{q_{x_t}(x_t)}[\ell(h(x_t), \tilde{f}_t(x_t))] + \rho_{11}^t (R_t(h, f_t) + \rho_{01}^s M_t). \quad (20)$$

Thus, we have

$$\begin{aligned} |\tilde{R}_t^{\text{po}}(h, \tilde{f}_t, u_t) - R_t(h, f_t)| &= |\rho_{01}^t \mathbb{E}_{q_{x_t}(x_t)}[\ell(h(x_t), \tilde{f}_t(x_t))] + \rho_{11}^t \mathbb{E}_{p'_{x_t}(x_t)}[\ell(h(x_t), f_t(x_t))] \\ &\quad - R_t(h, f_t)| \\ &\leq |\rho_{01}^t \mathbb{E}_{q_{x_t}(x_t)}[\ell(h(x_t), \tilde{f}_t(x_t))] + \rho_{11}^t (R_t(h, f_t) + \rho_{01}^s M_t) \\ &\quad - R_t(h, f_t)| \\ &= |\rho_{01}^t (\mathbb{E}_{q_{x_t}(x_t)}[\ell(h(x_t), \tilde{f}_t(x_t))] - R_t(h, f_t)) + \rho_{11}^t \rho_{01}^s M_t| \\ &\leq \rho_{01}^t \max\{\mathbb{E}_{q_{x_t}(x_t)}[\ell(h(x_t), \tilde{f}_t(x_t))], R_t(h, f_t)\} + \rho_{11}^t \rho_{01}^s M_t. \end{aligned}$$

This lemma is proved.

Remark 4 In Lemma 2, the assumption $\mathbb{E}_{p'_{x_t}(x_t)}[\ell(h(x_t), f_t(x_t))] \leq R_t(h, f_t) + \rho_{01}^s M_t$ means that the expect risk restricted in B (i.e., $\mathbb{E}_{p'_{x_t}(x_t)}[\ell(h(x_t), f_t(x_t))]$) can represent the true risk $R_t(h, f_t)$ when ρ_{01}^s is small, where $B = \{x : \tilde{f}_t(x) = f_t(x)\}$. In Butterfly, it is equivalent to that pseudo labels provided by noisy source data are more useful if we can select more correct data from noisy source data. If this assumption fails, we cannot gain useful knowledge from \tilde{f}_t even when we can perfectly select correct data from pseudo-labeled target data ($\rho_{01}^s = 0$).

Inequalities (16), (17) and (18) show that if we can avoid to annotate incorrect data as “correct” ($\rho_{01}^s = 0$ and $\rho_{01}^t = 0$), we have $\tilde{R}_s^{\text{po}}(h, u_s) = R_s(h)$, $\tilde{R}_t^{\text{po}}(h, \tilde{f}_t, u_t) = R_s(h, \tilde{f}_t)$ and $\tilde{R}_t^{\text{po}}(h, \tilde{f}_t, u_t) = R_t(h, f_t)$. Nonetheless, ρ_{01}^s and ρ_{01}^t never equal 0, and $\mathbb{E}_{q_s(x_s, y_s)}[\ell(h(x), y)]$, $\mathbb{E}_{q_{x_s}(x_s)}[\ell(h(x_s), \tilde{f}_t(x_s))]$ and $\mathbb{E}_{q_{x_t}(x_t)}[\ell(h(x_t), \tilde{f}_t(x_t))]$ may equal $+\infty$ for some h . In next section, we prove that, under the assumption in Remarks 1 and 2, $\tilde{R}_s^{\text{po}}(h, u_s) \rightarrow R_s(h)$, $\tilde{R}_s^{\text{po}}(h, \tilde{f}_t, u_t) \rightarrow R_s(h, \tilde{f}_t)$ and $\tilde{R}_t^{\text{po}}(h, \tilde{f}_t, u_t) \rightarrow R_t(h, f_t)$ if $\rho_{01}^s \rightarrow 0$ and $\rho_{01}^t \rightarrow 0$. Moreover, we give a new upper bound of $R_t(h, f_t)$.

Proof of Theorem 3 Now, we prove Theorem 3 as follows.

Proof. We first prove upper bounds of $|\tilde{R}_s^{\text{po}}(h, u_s) - R_s(h)|$, $|\tilde{R}_s^{\text{po}}(h, \tilde{f}_t, u_t) - R_s(h, \tilde{f}_t)|$ and $|\tilde{R}_t^{\text{po}}(h, \tilde{f}_t, u_t) - R_t(h, \tilde{f}_t)|$ under assumptions in Theorem 3.

Based on Lemma 1, we have

$$\begin{aligned} |\tilde{R}_s^{\text{po}}(h, u_s) - R_s(h)| &= |\rho_{01}^s \mathbb{E}_{q_s(x_s, y_s)}[\ell(h(x_s), y_s)] - (1 - \rho_{11}^s)R_s(h)| \\ &\leq |\rho_{01}^s(R_s(h) + M_s) - \rho_{01}^s R_s(h)| \\ &= \rho_{01}^s M_s. \end{aligned}$$

Similar, we have

$$|\tilde{R}_s^{\text{po}}(h, \tilde{f}_t, u_t) - R_s(h, \tilde{f}_t)| \leq \rho_{01}^t M_t,$$

$$|\tilde{R}_t^{\text{po}}(h, \tilde{f}_t, u_t) - R_t(h, \tilde{f}_t)| \leq \rho_{01}^t M_t + \rho_{11}^t \rho_{01}^s M_t.$$

Since M_s and M_t are positive constants, it is clear that $\tilde{R}_s^{\text{po}}(h, u_s) \rightarrow R_s(h)$, $\tilde{R}_s^{\text{po}}(h, \tilde{f}_t, u_t) \rightarrow R_s(h, \tilde{f}_t)$ and $\tilde{R}_t^{\text{po}}(h, \tilde{f}_t, u_t) \rightarrow R_t(h, \tilde{f}_t)$ when $\rho_{01}^s \rightarrow 0$ and $\rho_{01}^t \rightarrow 0$.

Specifically, $\forall \epsilon \in (0, 1)$, let $\delta_t = \epsilon/M_t$ and $\delta_s = \epsilon/\max\{M_s, \rho_{11}^t M_t\}$. When $\rho_{01}^s < \delta_s$ and $\rho_{01}^t < \delta_t$, we have

$$|\tilde{R}_s^{\text{po}}(h, u_s) - R_s(h)| + |\tilde{R}_s^{\text{po}}(h, \tilde{f}_t, u_t) - R_s(h, \tilde{f}_t)| < 2\epsilon$$

$$|\tilde{R}_t^{\text{po}}(h, \tilde{f}_t, u_t) - R_t(h, \tilde{f}_t)| < 2\epsilon.$$

Hence, we prove the Eq. (5). In following, we give a new upper bound of $R_t(h, f_t)$. Call back to Theorem 2, we replace 1) $\tilde{R}_s(h)$ with $\tilde{R}_s^{\text{po}}(h, u_s)$, 2) $\tilde{R}_s(h, \tilde{f}_t)$ with $\tilde{R}_s^{\text{po}}(h, \tilde{f}_t, u_t)$, 3) $R_s(h, \tilde{f}_t)$ with $\tilde{R}_t^{\text{po}}(h, \tilde{f}_t, u_t)$. Then, we have

$$\begin{aligned} R_t(h, f_t) &\leq \tilde{R}_s^{\text{po}}(h, u_s) + |\tilde{R}_t^{\text{po}}(h, \tilde{f}_t, u_t) - \tilde{R}_s^{\text{po}}(h, \tilde{f}_t, u_t)| + |R_s(h, \tilde{f}_t) - R_s(h)| \\ &\quad + |\tilde{R}_s^{\text{po}}(h, u_s) - R_s(h)| + |\tilde{R}_s^{\text{po}}(h, \tilde{f}_t, u_t) - R_s(h, \tilde{f}_t)| + |R_t(h, f_t) - \tilde{R}_t^{\text{po}}(h, \tilde{f}_t, u_t)|. \end{aligned}$$

Let $\rho_{01}^s \leq \delta_s$ and $\rho_{01}^t \leq \delta_t$, we have

$$\begin{aligned} R_t(h, f_t) &\leq \underbrace{\tilde{R}_s^{\text{po}}(h, u_s)}_{(i) \text{ risk on noisy data}} + \underbrace{|\tilde{R}_t^{\text{po}}(h, \tilde{f}_t, u_t) - \tilde{R}_s^{\text{po}}(h, \tilde{f}_t, u_t)|}_{(ii) \text{ discrepancy between distributions}} + \underbrace{|R_s(h, \tilde{f}_t) - R_s(h)|}_{(iii) \text{ domain dissimilarity}} \\ &\quad + \underbrace{2\epsilon}_{(iv) \text{ noise effects from source } \Delta_s} + \underbrace{2\epsilon}_{(v) \text{ noise effects from target } \Delta_t}, \end{aligned}$$

Hence, we prove this theorem.